OPEN ACCESS
CellPress

Cell Reports
Article

3′ UTR-Dependent, miR-92-Mediated Restriction of Tis21 Expression Maintains Asymmetric Neural Stem Cell Division to Ensure Proper Neocortex Size

Ji-Feng Fei,[1,2] Christiane Haffner,[1] and Wieland B. Huttner[1,*]
[1]Max Planck Institute of Molecular Cell Biology and Genetics, Pfotenhauerstrasse 108, 01307 Dresden, Germany
[2]Present address: Center for Regenerative Therapies Dresden, Technische Universität Dresden, Fetscherstrasse 105, 01307 Dresden, Germany
*Correspondence: huttner@mpi-cbg.de
http://dx.doi.org/10.1016/j.celrep.2014.03.033
This is an open access article under the CC BY-NC-ND license (http://creativecommons.org/licenses/by-nc-nd/3.0/).

SUMMARY

Mammalian neocortex size primarily reflects the number and mode of divisions of neural stem and progenitor cells. Cortical stem cells (apical progenitors) switching from symmetric divisions, which expand their population, to asymmetric divisions, which generate downstream neuronal progenitors (basal progenitors), start expressing Tis21, a so-called antiproliferative/prodifferentiative gene. Tis21 encodes a small (17.5 kDa), functionally poorly characterized protein and a relatively large (2 kb), highly conserved 3′ UTR. Here, we show that mice lacking the Tis21 3′ UTR develop a microcephalic neocortex with fewer neurons, notably in the upper layers. This reflects a progressive decrease in basal progenitors, which in turn is due to a fraction of apical progenitors prematurely switching from asymmetric self-renewing to symmetric self-consuming divisions. This switch is caused by the markedly increased Tis21 protein level resulting from lack of microRNA-, notably miR-92-, dependent restriction of Tis21 expression. Our data show that a premature onset of consumptive neural stem cell divisions can lead to microcephaly.

INTRODUCTION

Organ size is primarily determined by the number and mode of divisions that the relevant somatic stem cells (SCs) undergo during development. Symmetric proliferative divisions of SCs, where both daughter cells remain SCs, expand their population. The more often these divisions are repeated, the larger the SC pool will be. Asymmetric self-renewing divisions (ASDs) of SCs, where only one daughter is like the mother SC, on the one hand maintain (but do not increase) the size of the SC pool and on the other hand generate distinct progeny. The larger the SC pool, and the more often these divisions are repeated, the larger the production of such progeny will be. Divisions of SCs where neither daughter is like the mother SC, which can be symmetric or asymmetric depending on whether the daughter cells are identical or not, also generate distinct progeny but result in the consumption of the SC pool. The output of distinct progeny produced by this type of SC division is twice that of an ASD but is limited by the fact that due to its self-consuming nature, there can only be a single round of such cell division.

The mammalian brain, notably the neocortex (Ncx), is an organ where the molecular mechanisms that control the number and mode of somatic SC divisions during development are of particular interest. This is so not only because the Ncx is the site of higher cognitive functions, but also because its relative size is subject to dramatic changes during mammalian, and notably primate, evolution (Rakic, 2009). Thus, the size of the Ncx relative to that of other parts of the brain or to body size varies considerably between mammalian species. In recent years, substantial progress has been made in characterizing the neural stem and progenitor cells (NSPCs) that give rise to the neurons and glial cells of the Ncx (Borrell and Reillo, 2012; Fietz and Huttner, 2011; Götz and Huttner, 2005; Kriegstein and Alvarez-Buylla, 2009; Lui et al., 2011). Moreover, concepts about the evolutionary differences between mammalian species regarding the number and mode of neural stem cell (NSC) divisions during cortical development are beginning to emerge (Borrell and Reillo, 2012; Fietz and Huttner, 2011; Lui et al., 2011). However, little is known about the underlying molecular mechanisms.

Two principal classes of NSPCs generate the projection neurons of the Ncx. The first comprises the cells that undergo mitosis at the ventricular (that is, apical) surface of the cortical wall and that are collectively referred to as apical progenitors (APs). APs notably include neuroepithelial cells and the derivative apical radial glial cells (Fietz and Huttner, 2011; Götz and Huttner, 2005; Kriegstein and Alvarez-Buylla, 2009). These APs are NSCs, and their nuclei reside in the ventricular zone (VZ). The second class comprises cells that undergo mitosis at an abventricular location, typically in the subventricular zone (SVZ), and that are collectively referred to as basal progenitors (BPs) (Götz and Huttner, 2005). BPs include basal (or outer) radial glial cells, transit amplifying progenitors, and intermediate progenitor cells (IPCs) (Fietz and Huttner, 2011; Lui et al., 2011). Among the BPs, basal radial glial cells can be considered to be NSCs.

The development of the Ncx to different relative size in various mammalian species is thought to reflect differences not only in the number and mode of divisions of these distinct types of NSPCs but also in their relative abundance and lineage relationships (Borrell and Reillo, 2012; Fietz and Huttner, 2011; Lui et al., 2011). In the mouse and rat, the major lineage yielding cortical projection neurons, referred to as indirect neurogenesis, begins with APs switching from symmetric proliferative divisions to ASDs that generate a neurogenic BP as the other daughter. These BPs are IPCs that then undergo one round of symmetric consumptive division (SCD) that generates two neurons (Götz and Huttner, 2005; Kriegstein and Alvarez-Buylla, 2009). It follows that in this lineage, the number of cortical projection neurons originating from a given AP is determined by the number of ASDs this AP undergoes (Fietz and Huttner, 2011; Lui et al., 2011).

Mouse cortical APs switching from symmetric proliferative divisions to ASDs start to express Tis21 (Haubensak et al., 2004; Iacopetti et al., 1999), a member of the BTG/Tob or APRO protein family and reported to exert antiproliferative and prodifferentiative roles (Matsuda et al., 2001; Tirone, 2001). Tis21 then continues to be expressed in the BPs undergoing neurogenic SCD (Attardo et al., 2008; Haubensak et al., 2004). Although this temporal and spatial expression pattern is highly intriguing and has rendered Tis21 a powerful marker to identify neurogenic NSPCs (Attardo et al., 2008; Haubensak et al., 2004), little is known about the functional consequences of Tis21 expression in these cells for cortical neurogenesis and how this expression is regulated.

The regulation of gene expression is known to occur not only at the transcriptional level but also at the posttranscriptional level. Regarding the latter, the *Tis21* mRNA exhibits a remarkable feature: the presence of a 2 kb 3′ UTR, which is more than four times the size of the Tis21 protein-coding region (Bradbury et al., 1991; Fletcher et al., 1991). Importantly, the *Tis21* 3′ UTR is highly conserved across mammalian species (http://www.targetscan.org), suggesting functional significance. In the present study, we have investigated the relevance of the 3′ UTR for the regulation of *Tis21* mRNA and Tis21 protein levels in neurogenic APs and BPs of embryonic mouse brain. Our data reveal a key role of the *Tis21* 3′ UTR for Ncx size and the number of neurons generated during the development of the mouse Ncx. Specifically, the *Tis21* 3′ UTR, which is found to be a target of microRNAs, notably miR-92, regulates the Tis21 protein level, which in turn controls the mode of neurogenic AP division and thereby the level of neurogenic BPs.

RESULTS

The 3′ UTR of the *Tis21* mRNA Conveys Its Rapid Degradation

We initially explored a potential role of the 3′ UTR in the regulation of *Tis21* mRNA degradation in NIH 3T3 cells, in which *Tis21* mRNA can be induced by the phorbol ester TPA (Fletcher et al., 1991) (Tis, TPA-induced sequence). Using this system, we found that the 3′ UTR of the *Tis21* mRNA conveys its rapid degradation (Figures S1A–S1G and Supplemental Results).

Tis21 mRNA and Protein Are Upregulated in the Neocortical Germinal Zones of 3′ UTR Knockout Mouse Embryos

To assess the relevance of the 3′ UTR-mediated rapid degradation of the *Tis21* mRNA observed in vitro for the expression of Tis21 in the developing Ncx in vivo, and to determine the potential significance of an altered Tis21 expression for Ncx development, we generated a *Tis21* 3′ UTR knockout mouse line (from now on referred to as KO). In this mouse line, the entire 3′ UTR-encoding 2.0 kb portion of exon 2 of the *Tis21* gene was deleted and the *Tis21* open reading frame (ORF) was directly followed by a 250 bp SV40 polyadenylation signal (Figure 1A; for details, see Figures S1H–S1K).

Northern blot analysis of embryonic brains of wild-type (WT), heterozygous (het), and homozygous (hom) KO littermates at embryonic day 13.5 (E13.5), which corresponds to midneurogenesis in the embryonic mouse Ncx, revealed a much higher level (9-fold as determined in het embryos) of the *Tis21-Δ3′UTR* mRNA as compared to the *Tis21-fl* mRNA (Figure 1B). Because both the *Tis21-fl* mRNA and the *Tis21-Δ3′UTR* mRNA are transcribed under the control of the same 5′ promoter sequence (Figure 1A), the higher level of *Tis21-Δ3′UTR* mRNA presumably reflected, for the most part, a lower rate of degradation of this mRNA than the *Tis21-fl* mRNA.

Immunoblot analysis showed that the higher *Tis21* mRNA level observed upon 3′ UTR deletion resulted in a massive increase in Tis21 protein in the E13.5 brain (>10-fold in hom KO embryos) (Figure 1C). Consistent with the fact that *Tis21* is expressed in embryonic stem cells (ESCs) (Rouault et al., 1996), the het ESCs generated to produce the KO mouse line also showed drastically increased levels of *Tis21-Δ3′UTR* mRNA as compared to *Tis21-fl* mRNA (Figure S1L), and of Tis21 protein (Figure S1M), when compared with WT ESCs.

In situ hybridization (ISH) of E13.5 Ncx cryosections using an *ORF* antisense probe revealed that the *Tis21* mRNA was markedly upregulated in het (Figure 1F) and hom (Figure 1G) KO mice compared with WT littermates (Figures 1D and 1E; Figure S1O). As in WT (Figure 1E), expression of *Tis21* mRNA in KO embryos (Figures 1F and 1G) was restricted to the VZ and SVZ and absent in the cortical plate (CP). No ISH signal was obtained with E13.5 Ncx cryosections of hom KO mice when a 3′ UTR antisense probe was used, in contrast to WT and het KO littermates (Figures S1N and S1O).

3′ UTR-Mediated Downregulation of *Tis21* mRNA Requires MicroRNAs

We searched the *Tis21* 3′UTR for the possible occurrence of sequence elements known to promote mRNA degradation. Indeed, the *Tis21* 3′ UTR was found to harbor two Bearded boxes (Lai and Posakony, 1997) and five presumptive AU-rich elements (Chen and Shyu, 1995). Even more strikingly, however, the 3′ UTR of the *Tis21* mRNA, along its entire length, is predicted to be the target of many microRNAs (see Figure 3A), which are known mediators of mRNA degradation (Huntzinger and Izaurralde, 2011). Moreover, for two of these microRNAs (miR-21 and miR-32), experimental evidence for their role in regulating the Tis21 level has been obtained in nonneural cells in culture (Jalava et al., 2012; Yang et al., 2011). Given that microRNA

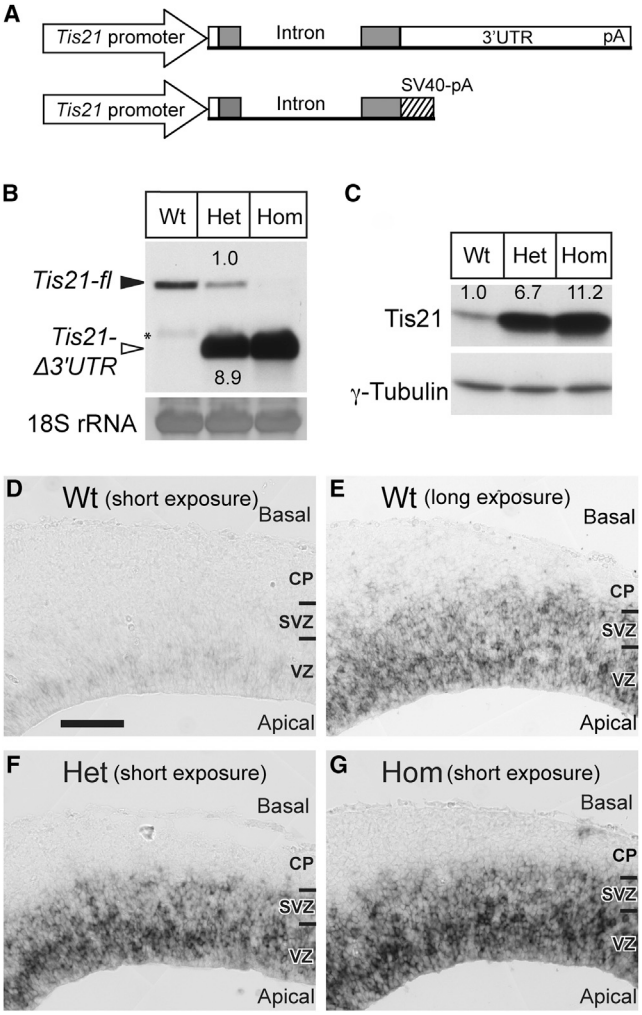

Figure 1. Increased Tis21 Expression in the Ncx Germinal Zones of 3′ UTR Knockout Mouse Embryos

(A) WT (top) and KO (bottom) *Tis21* alleles.

(B) Northern blot of *Tis21-fl* (solid arrowhead) and *Tis21-Δ3′UTR* (open arrowhead) mRNAs using total RNA from E13.5 brain of WT, het, and hom KO embryos. 18S rRNA, loading control. Numbers indicate the mean level of *Tis21-Δ3′UTR* mRNA relative to *Tis21-fl* mRNA in het brain as determined from two separate blots, with the *Tis21-fl* mRNA arbitrarily set to 1.0. Asterisk, 3′ UTR-truncated *Tis21* mRNA splice variants (see Figure S4C).

(C) Tis21 immunoblot of WT, het, and hom KO E13.5 brain (30 μg total protein). γ-Tubulin immunoblot, loading control. Numbers indicate the mean level of Tis21 in het and hom brain relative to WT as determined from two separate blots, with WT arbitrarily set to 1.0.

(D–G) *Tis21* mRNA ISH of littermate WT (D and E), het (F), and hom (G) KO E13.5 Ncx using an antisense *Tis21 ORF* RNA probe. Exposure time in (D), (F), and (G) is identical, whereas (E) shows a longer exposure of WT to reveal the normal pattern of *Tis21* mRNA expression in the VZ and SVZ; note the massive upregulation of *Tis21* mRNA in the VZ and SVZ of het and hom KO embryos, with the pattern being the same as WT. Scale bar in (D), 100 μm.

production requires the endoribonuclease Dicer (Murchison et al., 2005), we investigated the consequences of conditional Dicer ablation for Tis21 mRNA and protein levels in the E13.5 mouse cerebral cortex. Conditional Dicer ablation using *Emx1*-Cre (De Pietri Tonelli et al., 2008), which starts to be expressed in the developing mouse cerebral cortex as of E9.5, was performed in het *Tis21*-GFP knockin mice (Haubensak et al., 2004), which carry one WT *Tis21* allele and one *Tis21* allele from which *GFP* mRNA instead of *Tis21* mRNA is transcribed (Figure 2A).

In these mice, by E13.5, Dicer ablation in the dorsal telencephalon (d-Tel) giving rise to the Ncx and archicortex (Figure 2B) resulted in a ~2-fold increase in the *Tis21* mRNA level as revealed by northern blot analysis (Figure 2C). This increase likely reflected increased *Tis21* mRNA stability rather than its increased transcription, because the level of *GFP* mRNA, the transcription of which was under the control of the same *Tis21* 5′ promoter sequence (Figure 2A), was actually decreased rather than increased (Figure 2C). Immunoblot analysis of the Dicer-ablated E13.5 d-Tel of these mice showed that the increase in *Tis21* mRNA resulted in a ~4-fold higher level of Tis21 protein (Figure 2D). These data suggest that Dicer-generated microRNAs decrease the level of *Tis21* mRNA, and consequently Tis21 protein, in the developing cerebral cortex.

If microRNAs exert this effect via the 3′ UTR of the *Tis21* mRNA, then Dicer ablation should not result in an increase in *Tis21-Δ3′UTR* mRNA. Northern blot analysis of E13.5 d-Tel of het KO mice indicated that this was indeed the case, whereas the *Tis21-fl* mRNA was increased 2.3-fold compared with control (Figure 2E).

ISH of E13.5 Tel of het *Tis21*-GFP knockin mice showed that conditional Dicer ablation in the d-Tel using *Emx1*-Cre increased the expression of *Tis21* mRNA in the germinal zones of the Ncx and archicortex, but not of the lateral ganglionic eminence (Figure 2, compare panels G and F), which lacks *Emx1*-Cre expression (Figure 2B). In contrast, the expression of *GFP* mRNA in the germinal zones of the Ncx and archicortex was not increased but, if anything, appeared to be slightly decreased upon Dicer ablation (Figures 2H and 2I), consistent with the northern blot data (Figure 2C). Quantification of the ISH signal for *Tis21* mRNA relative to *GFP* mRNA revealed a 2-fold increase in Ncx and archicortex, but not lateral ganglionic eminence, upon Dicer ablation (Figure S2).

Identification of miR-92 as a Major Regulator of 3′ UTR-Dependent Tis21 Expression

To directly demonstrate the microRNA-dependent, *Tis21* 3′ UTR-mediated decrease in protein expression, we electroporated E13.5 dorsolateral telencephalon (dl-Tel) of WT mice with plasmids encoding *GFP* mRNA and monomeric red fluorescent protein (*mRFP*) mRNA, *mRFP* mRNA fused to the 2.0 kb *Tis21* 3′ UTR (*mRFP-3′UTR*), or *mRFP* mRNA fused to a mutated 1.9 kb *Tis21* 3′ UTR in which the core sequence (7–8 nt) of each of the 17 microRNA binding sites (Figure 3A) had been deleted (*mRFP-3′UTRmut*). Analysis of mRFP fluorescence relative to GFP fluorescence at E14.5 showed a 10-fold lower level when the *Tis21* 3′ UTR had been fused to the *mRFP* mRNA (Figures 3B and 3C, *mRFP* versus *mRFP-3′UTR*). This decrease was largely rescued when the microRNA binding sites in the *Tis21* 3′UTR had been deleted (Figures 3B and 3C, *mRFP-3′UTRmut*).

We sought to identify specific microRNA binding sites within the *Tis21* 3′ UTR that were of particular importance for the

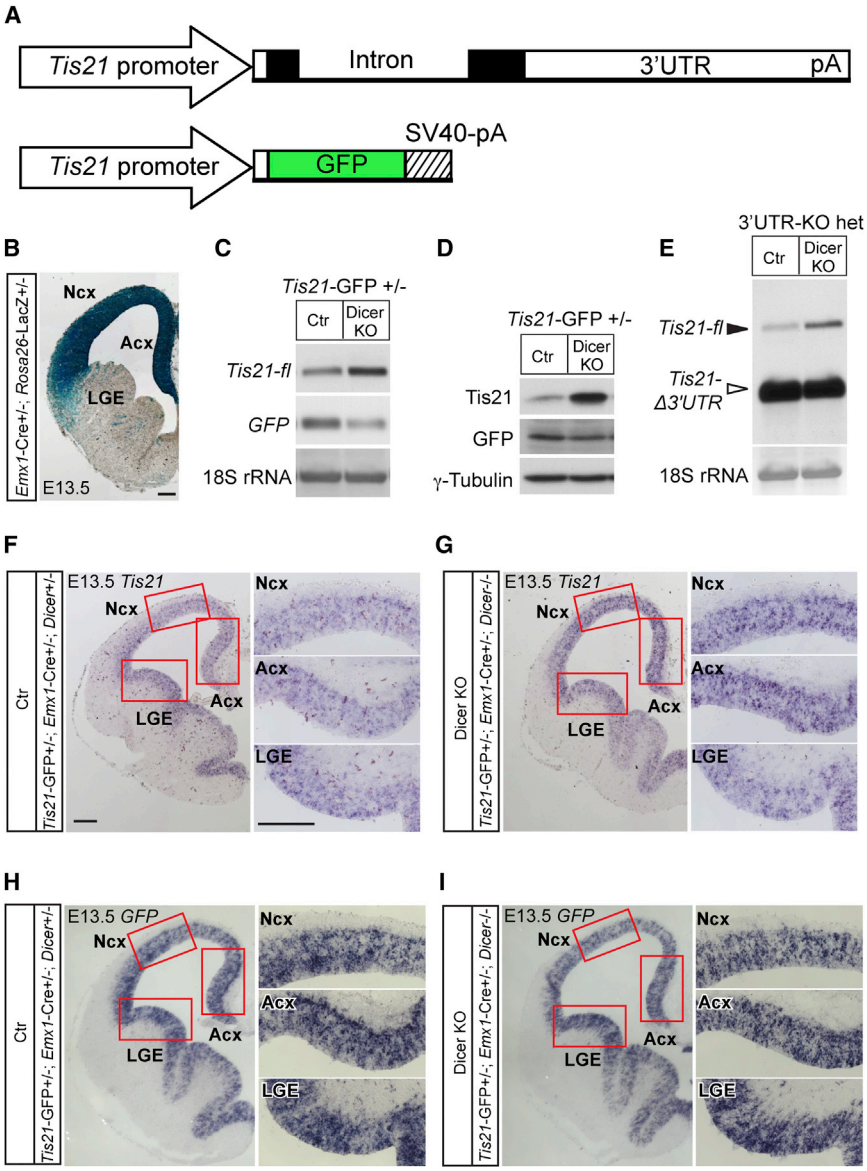

Figure 2. Increased Tis21 Expression in Embryonic Ncx in the Absence of MicroRNAs

(A) WT *Tis21* allele (top) and *Tis21*-GFP knockin allele (bottom).

(B) Coronal cryosection showing *Emx1*-Cre expression (blue) in E13.5 d-Tel of *Emx1*-Cre/*Rosa26*-LacZ mouse.

(C–I) Triple transgenic mouse embryos were as follows: (i) either $Tis21^{GFP/WT}$ (*Tis21*-$GFP^{+/-}$; C, D, and F–I) or $Tis21^{\Delta 3'UTR/WT}$ (3′ UTR-KO het, E), (ii) $Emx1^{Cre/WT}$ (*Emx1*-$Cre^{+/-}$), and (iii) either $Dicer^{wt/flox}$ (*Dicer*$^{+/-}$) as control (C, D, F, and H) or $Dicer^{flox/flox}$ (*Dicer*$^{-/-}$; C, D, G, and I).

(C and E) Northern blot of endogenous *Tis21-fl* (solid arrowhead in E), *GFP*, and *Tis21-Δ3′UTR* (open arrowhead in E) mRNAs using total RNA from E13.5 d-Tel of control and Dicer KO embryos. 18S rRNA, loading control.

(D) Immunoblot of Tis21 and GFP from E13.5 d-Tel (15 μg total protein) of control and Dicer KO embryos. γ-Tubulin immunoblot, loading control.

(F–I) *Tis21* (F and G) and *GFP* (H and I) mRNA ISH of littermate control (F and H) and Dicer KO (G and I) E13.5 Tel. Red boxes, areas shown at higher magnification on the right. (F) and (G), respectively (H) and (I), are identical exposures. Note the upregulation of *Tis21*, but not *GFP*, mRNA in the dorsal (Ncx and Acx), but not ventral (LGE), Tel in Dicer KO brain compared to control. Ctr, control; Acx, archicortex; LGE, lateral ganglionic eminence. Scale bars in (B) and (F), 250 μm.

decrease in protein expression. For reasons explained below (see Discussion), we focused on miR-92 and deleted the corresponding, twice-occurring 8 nt sequence from the *Tis21* 3′ UTR where miR-92 is predicted to bind (Figure 3A). When fused to *mRFP*, this mutated *Tis21* 3′ UTR (*mRFP-3′UTR-miR92mut*) yielded a similarly high mRFP/GFP fluorescence ratio after coelectroporation with *GFP* into dl-Tel as the *mRFP-3′UTRmut* construct in which all 17 microRNA binding sites had been deleted (Figures 3B and 3C). Moreover, the dramatic reduction in the mRFP/GFP fluorescence ratio observed upon fusion of the *Tis21* 3′ UTR to *mRFP* (*mRFP-3′UTR*) was essentially reverted by coelectroporation of a miR-92 inhibitor (Figures 3B and 3C, *mRFP-3′UTRmut+miR92-inh*), but not of a microRNA inhibitor control (Figures 3B and 3C, *mRFP-3′UTRmut+ctr*). These data identify miR-92 as a major regulator of Tis21 expression, acting via the *Tis21* 3′ UTR.

KO Mice Develop Microcephaly

In light of the upregulation of Tis21 in the Ncx germinal zones of KO embryos (Figures 1M and 1N) and the known expression of Tis21 in all areas of the embryonic mouse brain in correlation with neurogenesis (Haubensak et al., 2004; Iacopetti et al., 1999), we explored the possible consequences for brain development. Adult brains of het, and even more so hom, KO mice appeared to show a decrease in overall size (Figures 4A–4C and 4A′–4C′) and exhibited a reduction in radial thickness of the Ncx (12% in hom) (Figures 4A″–4C″). Quantification of brain weight indeed revealed an ~8% and ~13% reduction, respectively (Figure 4D). We analyzed DAPI-stained coronal vibratome sections, obtained at three distinct positions along the rostral-to-caudal axis, to determine the area of the whole brain, the Ncx, and the brain without Ncx (Figures 4E–4E″). The decrease in total brain area in the het and hom KO mice (Figure 4F) was very similar to that in brain weight (Figure 4D). Interestingly, the decrease in Ncx area in the het and hom KO mice (Figure 4G) was consistently greater (up to 17%) than that observed for the brain without Ncx (up to 10%; Figure 4H).

The microcephaly observed for adult KO mice had its roots in the embryonic development of the brain. We immunostained the Tel of E16.5 embryos (i.e., at late neurogenesis in the Ncx) for the

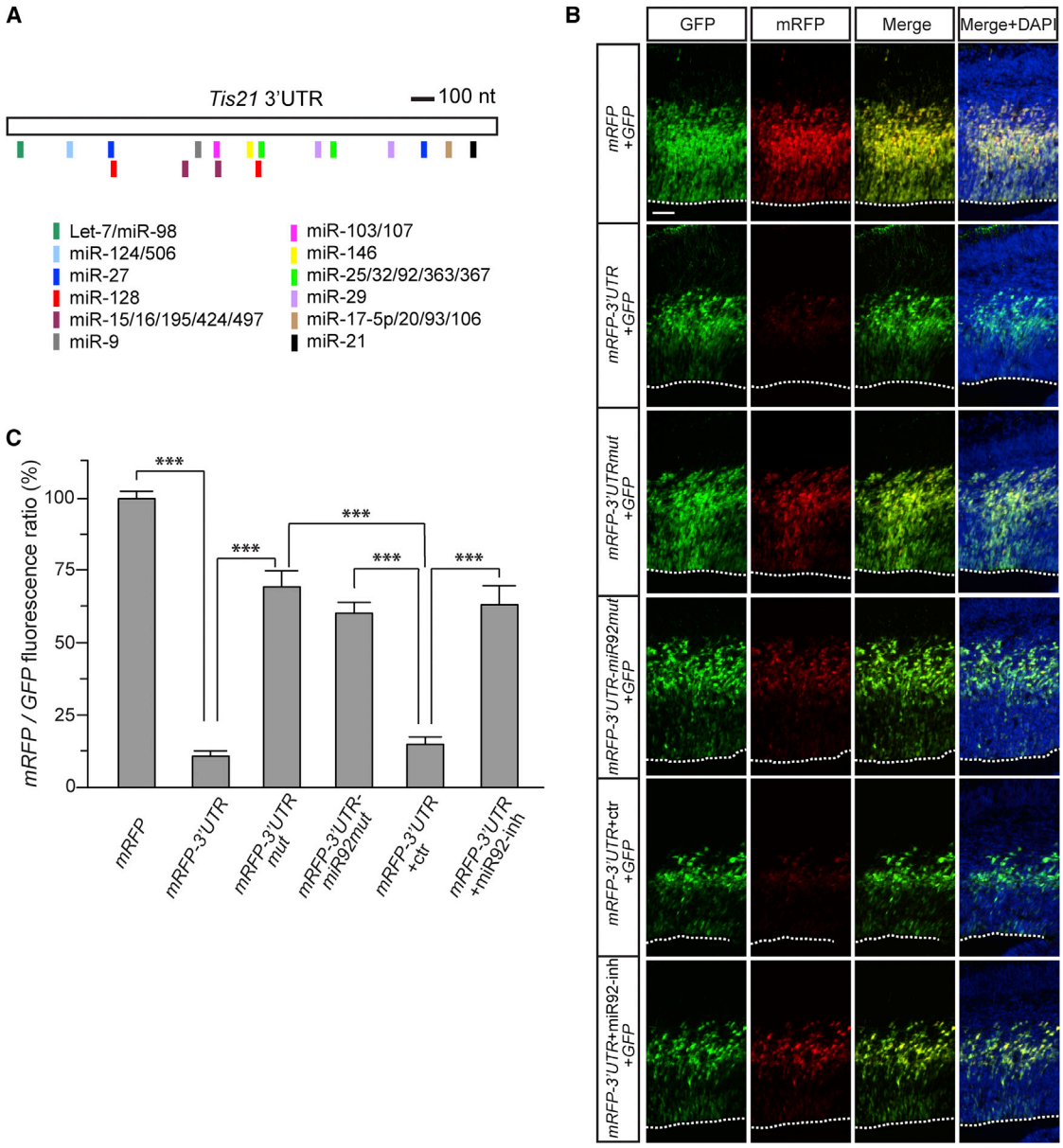

Figure 3. *Tis21* 3′ UTR Mediates a MicroRNA-, Notably miR-92-, Dependent Decrease in Gene Expression in Embryonic Ncx

(A) Location of putative microRNA binding sites in the *Tis21* 3′ UTR.

(B) dI-Tel of E13.5 WT embryos was coelectroporated with pCAGGS-*EGFP* combined with either pCAGGS-*mRFP* (row 1), pCAGGS-*mRFP-3′UTR* (row 2), pCAGGS-*mRFP-3′UTRmut* (row 3), pCAGGS-*mRFP-3′UTR-miR-92mut* (row 4), pCAGGS-*mRFP-3′UTR* + microRNA inhibitor control (ctr) (row 5), or pCAGGS-*mRFP-3′UTR* + miR-92 inhibitor (miR-92-inh) (row 6) and analyzed 24 hr later for GFP (green) and mRFP (red) fluorescence and DAPI staining (blue) on 10 μm coronal cryosections. Scale bar, 50 μm.

(C) Quantification of mRFP fluorescence relative to GFP fluorescence as shown in (B). Data are the mean of five fields each (one field per cryosection, one or two cryosections per embryo, three embryos from two litters per condition) and are expressed as ratio of mRFP/GFP fluorescence, with the ratio obtained in the case of the *mRFP* + *GFP* constructs (*mRFP*) being set to 100% and the ratios obtained in the other five cases being expressed relative to this. Columns from left to right in (C) correspond to rows from top to bottom in (B). Error bars, SEM; ***$p < 0.001$.

cortical layer markers FoxP2 and Satb2 (Molyneaux et al., 2007) to reveal the lateral and radial extension of the Ncx (Figures 5A and S3A) and for βIII-tubulin to reveal the thickness of the CP (Figure 5B). Hom KO embryos showed a significant (~10%) decrease in the mean radial thickness of the Ncx (Figure 5C), which was primarily due to a reduction in the thickness of the CP (Figure 5B). By comparison, we found a lesser (<5%) reduction in the size of the Ncx in the lateral dimension and only for the pial (Figure 5E), but not ventricular (Figure 5D), surface. Together, these data raised the possibility that the microcephaly observed

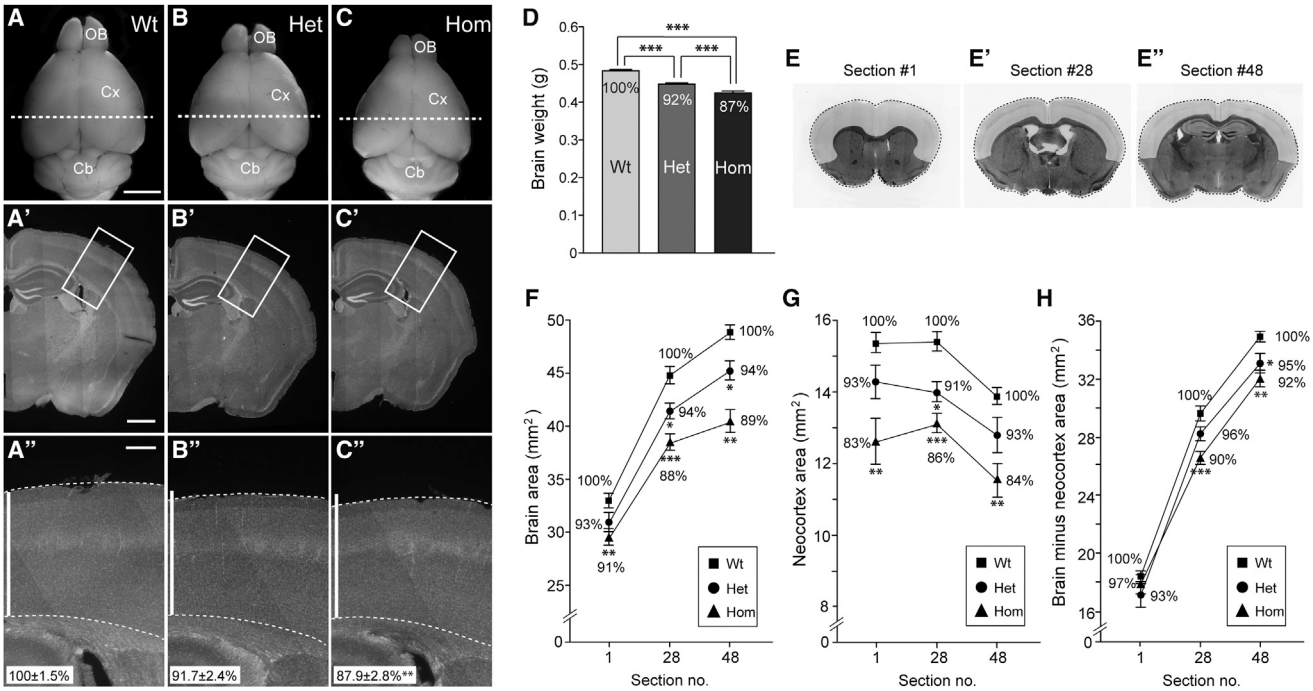

Figure 4. Adult KO Mice Exhibit Reduced Ncx Size

(A–C″) Brain and Ncx of adult (9 weeks old) WT, het, and hom KO littermates. OB, olfactory bulb; Cx, cortex; Cb, cerebellum. White dotted lines in (A–C), approximate position of DAPI-stained 50 μm vibratome coronal sections shown in (A′–C′). Areas in white boxes in (A′–C′) are shown at higher magnification in (A″–C″). White dashed lines in (A″–C″), cytoarchitectonic boundaries of Ncx. White vertical bar in (A″) indicates radial thickness of WT Ncx and is copied to (B″) and (C″) to allow comparison with radial thickness of KO Ncx; note the stepwise reduction in radial thickness in het (B″) and hom (C″) KO Ncx compared to WT. Numbers in (A″–C″) are mean radial thickness of five determinations each (four mice each, one or two vibratome sections per mouse), with the mean WT value set to 100% and the mean het and hom values expressed relative to this; ±SEM; $^{**}p < 0.01$. Scale bars, 3 mm in (A), 1 mm in (A′), 200 μm in (A″).

(D) Brain weight of adult (9–13 weeks old) WT (light gray), het (dark gray), and hom (black) KO mice. Mean of 36 (WT), 34 (het), and 15 (hom) determinations; error bars, SEM; $^{***}p < 0.001$. Numbers: mean WT value was set to 100%, and mean het and hom values were expressed relative to this.

(E–E″) Images of three representative DAPI-stained (color-inverted) 50 μm coronal vibratome sections along the rostral-caudal axis of WT adult brain at positions #1, #28, and #48, illustrating the quantification of brain area (dotted line, F), Ncx area (light gray, G), and brain area minus Ncx area (H).

(F–H) Quantification of brain area (F), Ncx area (G), and brain area minus Ncx area (H) on sections #1, #28, and #48 of adult (9 weeks old) WT (squares), het (circles), and hom (triangles) KO mice. Ordinates are truncated by a similar proportion (~40%). Mean of six (WT), five (het), and eight (hom) determinations; error bars, SEM; $^{*}p < 0.05$, $^{**}p < 0.01$, $^{***}p < 0.001$. Numbers on curves: at each section, the mean WT value was set to 100%, and the mean het and hom values were expressed relative to this.

for adult KO mice may be primarily due to a decrease in embryonic neurogenesis, i.e., in the Tis21-positive NSPCs, which generate neurons via asymmetric and symmetric neurogenic divisions largely in a radial manner (Attardo et al., 2008; Haubensak et al., 2004; Kowalczyk et al., 2009), rather than in Tis21-negative NSPCs, the symmetric proliferative divisions of which are thought to underlie the lateral expansion of the rodent Ncx.

KO Mice Exhibit Reduced Cortical Neurogenesis

To explore this possibility, we quantified deep-layer and upper-layer neurons in the postnatal day 0.5 (P0.5) Ncx, which like the E16.5 and adult Ncx showed a reduction in overall size and radial thickness (14%) in hom KO compared to WT mice (Figures 5F–5G″). Immunostaining for Tbr1 and FoxP2 (Figures 5H and 5I), two markers of deep-layer neurons (Molyneaux et al., 2007), and for Satb2 and Brn1 (Figures 5J and 5K), two markers of upper-layer neurons (Molyneaux et al., 2007), revealed a 10%–14% (Figures 5L and 5M) and 20%–22% (Figures 5N and 5O) reduction, respectively, in the P0.5 hom KO Ncx. Thus, the upregulation of Tis21 in the Ncx germinal zones of KO embryos (Figures 1M and 5N) has a greater impact on late-born than early-born neurons.

This conclusion was further corroborated by quantification of deep-layer and upper-layer neurons in the E16.5 Ncx. Whereas the decrease in Tbr1-expressing neurons in hom KO compared to WT mice was already as great as that found at P0.5 (Figures S3B and S3C, compare with Figure 5L), that in Satb2-expressing neurons had not yet reached the same extent as observed at P0.5 (Figures S3B and S3D, compare with Figures 5N and 5Q).

TUNEL staining indicated that the reduction in cortical neurons in KO embryos was not due to increased apoptosis in the germinal zones or in the CP (Figure S3E), which implies that this reduction reflected a decrease in neurogenesis. To corroborate a reduced rate of neurogenesis in the embryonic KO Ncx, we labeled NSPCs with a single pulse of bromodeoxyuridine (BrdU)

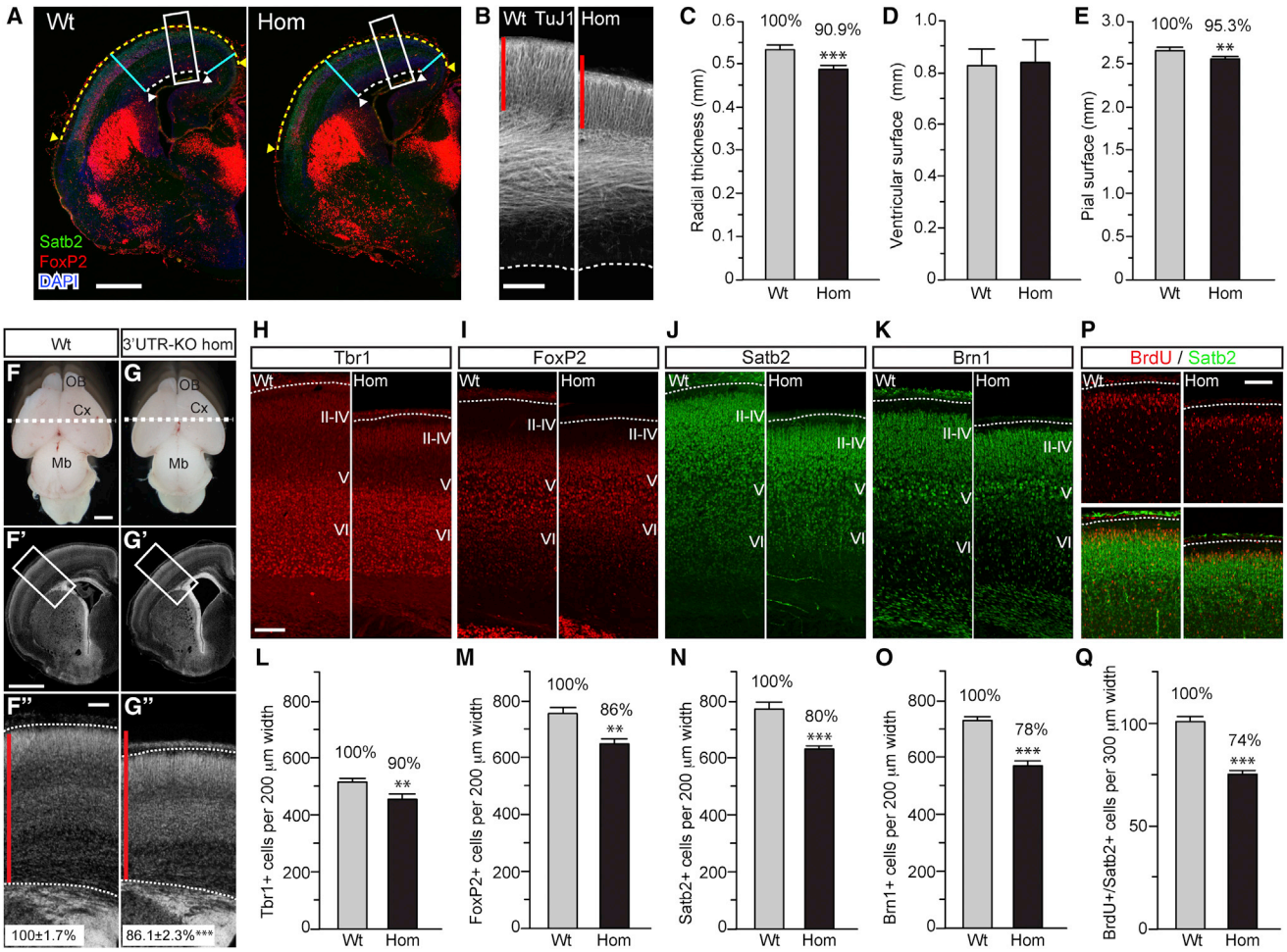

Figure 5. Cortical Neurons, Notably in Upper Layers, Are Reduced in KO Mice

(A–E) Radial thickness of Ncx is reduced in E16.5 KO mice.

(A) Double immunofluorescence (IF) for Satb2 (green) and FoxP2 (red) combined with DAPI staining (blue) on 10 μm coronal cryosections of E16.5 Tel of WT and hom KO littermates. Yellow dashed line and triangles, pial surface of Ncx (see E); white dashed line and triangles, ventricular surface of Ncx (see D); turquoise lines, radial thickness of Ncx at the lateral-most and medial-most positions quantified (see C). White boxes, areas for which a separate βIII-tubulin immunostaining at higher magnification is shown in (B). Scale bar, 500 μm.

(B) βIII-Tubulin IF on 10 μm coronal cryosections of E16.5 dl-Tel of WT and hom KO littermates. Red bar in (B, left panel) indicates the radial thickness of the WT CP and is copied to (B, right panel) to allow comparison with the radial thickness of the hom KO CP. Dashed line, ventricular surface. Scale bar, 100 μm.

(C–E) Quantification of radial thickness (C), ventricular surface (D), and pial surface (E), as described in (A); gray, WT; black, hom. Mean of six (C; WT, hom) cryosections from three littermates each and of 32 (D and E; WT) and 34 (D and E; hom) cryosections from four embryos each of three litters; error bars, SEM; **$p < 0.01$, ***$p < 0.001$. Numbers above columns in (C) and (E): mean WT value was set to 100%, and mean hom value is expressed relative to this.

(F–Q) Cortical neurons, notably in upper layers, are reduced in newborn KO mice.

(F–G″) Brain and Ncx of P0.5 WT and hom KO littermates. OB, olfactory bulb; Cx, cortex; Mb, midbrain. White dotted lines in (F) and (G), approximate position of DAPI-stained 50 μm vibratome coronal sections shown in (F′) and (G′). Areas in white boxes in (F′) and (G′) are shown at higher magnification in (F″) and (G″) (bright-field epifluorescence). White dotted lines in (F″) and (G″), cytoarchitectonic boundaries of Ncx. Red vertical bar in (F″) indicates radial thickness of WT Ncx and is copied to (G″) to allow comparison with radial thickness of KO Ncx; note the reduction in Ncx thickness in hom KO mice. Numbers in (F″) and (G″), mean radial thickness of eight determinations each (four mice each, two vibratome sections per mouse), with mean WT value set to 100% and mean hom value expressed relative to this; ±SEM; ***$p < 0.001$. Scale bars, 1 mm in (F) and (F′) and 100 μm in (F″).

(H–K) IF for Tbr1 (H, red), FoxP2 (I, red), Satb2 (J, green), and Brn1 (K, green) on 50 μm coronal vibratome sections (10 μm optical sections) of P0.5 Ncx of WT (left panels) and hom KO (right panels) littermates. (H) and (J), respectively (I) and (K), are double IF on the same vibratome sections. Roman numbers, cortical layers; dotted lines, basal boundary of CP neuronal nuclei. Scale bar, 100 μm in (H).

(L–O) Quantification of nuclei being Tbr1+ in layers V–VI (L), FoxP2+ in layers IV–VI (M), Satb2+ in layers II–VI (N), and Brn1+ in layers II–VI (O), in each case in a 200-μm-wide field of P0.5 Ncx of WT (gray) and hom KO (black) littermates. Mean of eight determinations each (four mice each, two vibratome sections per mouse).

(P) WT (left) and hom KO (right) E16.5 littermates were labeled by a single pulse of BrdU in utero, followed at P0.5 by double IF for BrdU (red, top and bottom) and Satb2 (green, bottom) on 50 μm coronal vibratome sections (10 μm optical sections) of Ncx. Dotted lines, basal boundary of CP neuronal nuclei. Scale bar, 100 μm.

(legend continued on next page)

at E16.5 and quantified, at P0.5, the Satb2-positive cortical neurons that had been generated from these NSPCs (Figure 5P). The 26% reduction observed (Figure 5Q) confirmed that there was a significant decrease in neurogenesis in the embryonic hom KO Ncx.

APs and BPs Are Reduced in the KO Ncx at Late-Stage Neurogenesis

The expression of Tis21 in the VZ and SVZ of the embryonic mouse Ncx is known to reflect its expression specifically in neurogenic APs, that is, APs that divide asymmetrically to self-renew and generate either a neuron or a neurogenic BP (that is, an IPC) as the other daughter cell, and in neurogenic BPs, which divide symmetrically to generate two neurons (Attardo et al., 2008; Haubensak et al., 2004). The upregulation of Tis21 expression in the germinal zones of KO mice (Figures 1M and 1N) therefore implied its upregulation specifically in neurogenic APs and BPs. In light of the decrease in neurogenesis in the embryonic KO Ncx, we therefore investigated whether this upregulation resulted in a reduction in these NSPCs in KO embryos. APs were identified by the marker Pax6 (Englund et al., 2005) or by mitosis occurring at the ventricular (apical) surface and BPs by the marker Tbr2 (Englund et al., 2005) or by mitosis occurring in the basal half of the VZ or in the SVZ. We assumed that any reduction in APs and/or BPs would pertain only to the neurogenic, Tis21-expressing subpopulations of these NSPCs.

At E10.5 (i.e., the onset of neurogenesis), no differences in the number of APs or BPs were observed between WT and hom KO Ncx (Figures 6B and 6E–6H). The same was the case for APs at midneurogenesis (E13.5) (Figures 6C, 6E, and 6G). At this stage, however, BPs already showed a small, albeit not statistically significant, reduction in number in hom KO Ncx when compared to WT, when quantifying Tbr2-positive cells in both the VZ plus SVZ (Figures 6C and 6F) and basal mitoses (Figures 6C and 6H). Consistent with a beginning reduction in BPs, microarray analysis of total RNA of E13.5 brain revealed a significant (35%) reduction in *Tbr2* mRNA in hom KO embryos when compared to WT (data not shown). Remarkably, at E16.5 (i.e., late neurogenesis), both APs and BPs were significantly reduced in hom KO Ncx, with the decrease being greater for BPs (23%–33%) than for APs (13%–18%) (Figures 6D and 6E–6H). Previous studies suggest that approximately half of the APs at E16.5 are Tis21 positive (Arai et al., 2011; Haubensak et al., 2004). Given that the effects of Tis21 upregulation in APs are confined to the Tis21-positive subpopulation, the 13% decrease in Pax6-positive cells in the VZ (Figure 6E) and the 18% decrease in apical mitoses (Figure 6G) thus reflected a reduction in neurogenic APs by about one-quarter to one-third, respectively. This reduction was very similar in magnitude to that observed for Tbr2-positive cells in E16.5 VZ plus SVZ (Figure 6F) and basal mitoses (Figure 6H), i.e., in BPs, ~90% of which are known to be Tis21 positive (Arai et al., 2011; Haubensak et al., 2004).

Tis21 Upregulation in Neurogenic NSPCs Does Not Lengthen Their Cell Cycle

There are several possible explanations, which are not mutually exclusive, for the reduced levels of neurogenic NSPCs at late neurogenesis in KO Ncx due to the upregulation of Tis21. Given the antiproliferative function reported for Tis21 (Matsuda et al., 2001; Tirone, 2001), one is that Tis21 upregulation lengthens, or even arrests, the cell cycle of the APs concerned. This would result in a reduced number of apical mitoses, as observed (Figure 6G), and in a reduced generation of BPs, which in turn would result in the observed decrease in the level of BPs (Figure 6F) and basal mitoses (Figure 6H).

We investigated a possible effect of Tis21 upregulation on the cell cycle of APs by cumulative BrdU labeling (Arai et al., 2011) of E14.5 mice carrying one *Tis21* allele expressing GFP rather than Tis21 protein and either one *Tis21* WT allele (as control) or one *Tis21* 3′ UTR KO allele (Figure 7A). These mice showed increased Tis21 expression at E13.5 (Figure 7B) and reduced adult brain weight (Figure 7C). Analysis of the NSPCs in the VZ that lack Tis21 expression (Figure 7D) showed that all their cell-cycle parameters as well as their growth fraction were virtually indistinguishable between control and KO Ncx (Figure 7E). These results were expected given the lack of Tis21 expression in these NSPCs. Remarkably, however, cumulative BrdU labeling also showed that the Tis21-expressing NSPCs in the VZ (Figure 7D) exhibited the same cell-cycle parameters between control and KO Ncx (Figure 7F). Moreover, the identical growth fraction of >90% of the Tis21-GFP-positive NSPCs in the VZ in WT and KO Ncx also indicates that the increased Tis21 expression due to 3′ UTR deletion does not cause cell-cycle exit of APs. These data (see also the Supplemental Results) therefore eliminate cell-cycle lengthening or arrest in the Tis21-overexpressing APs as a possible explanation for the reduced levels of neurogenic NSPCs at late neurogenesis in KO embryos.

Tis21 Upregulation in APs of KO Ncx Results in Their Switching from Asymmetric Self-Renewing to Symmetric Consumptive Division

Another possible explanation for the reduced levels of neurogenic NSPCs at late neurogenesis in KO Ncx is that the Tis21 upregulation in neurogenic APs alters their mode of cell division with regard to the fate of the resulting daughter cells such that the levels of neurogenic NSPCs become reduced. Typically, most Tis21-expressing neocortical APs undergo BP-genic ASD, that is, an AP mother gives rise to an AP daughter plus a neurogenic BP daughter (Attardo et al., 2008; Haubensak et al., 2004). We explored the possibility that upon Tis21 overexpression due to the deletion of the *Tis21* 3′ UTR, some APs may switch to BP-genic SCD, with both daughter cells becoming neurogenic BPs. This would lead to a progressive depletion of APs undergoing BP-genic ASD and, as a consequence, eventually to a reduction in the neurogenic BP pool size and hence the number of neurons produced. To this end, we electroporated

(Q) Quantification of BrdU and Satb2 double-positive nuclei in layers II–VI in a 300-μm-wide field of P0.5 Ncx of WT (gray) and hom KO (black) littermates BrdU-labeled at E16.5 as in (K). Mean of ten determinations each (two mice each, five vibratome sections per mouse).
(L–O and Q) Error bars, SEM; $^{**}p < 0.01$, $^{***}p < 0.001$. Numbers above columns: for each marker, mean WT value was set to 100%, and mean hom value is expressed relative to this.

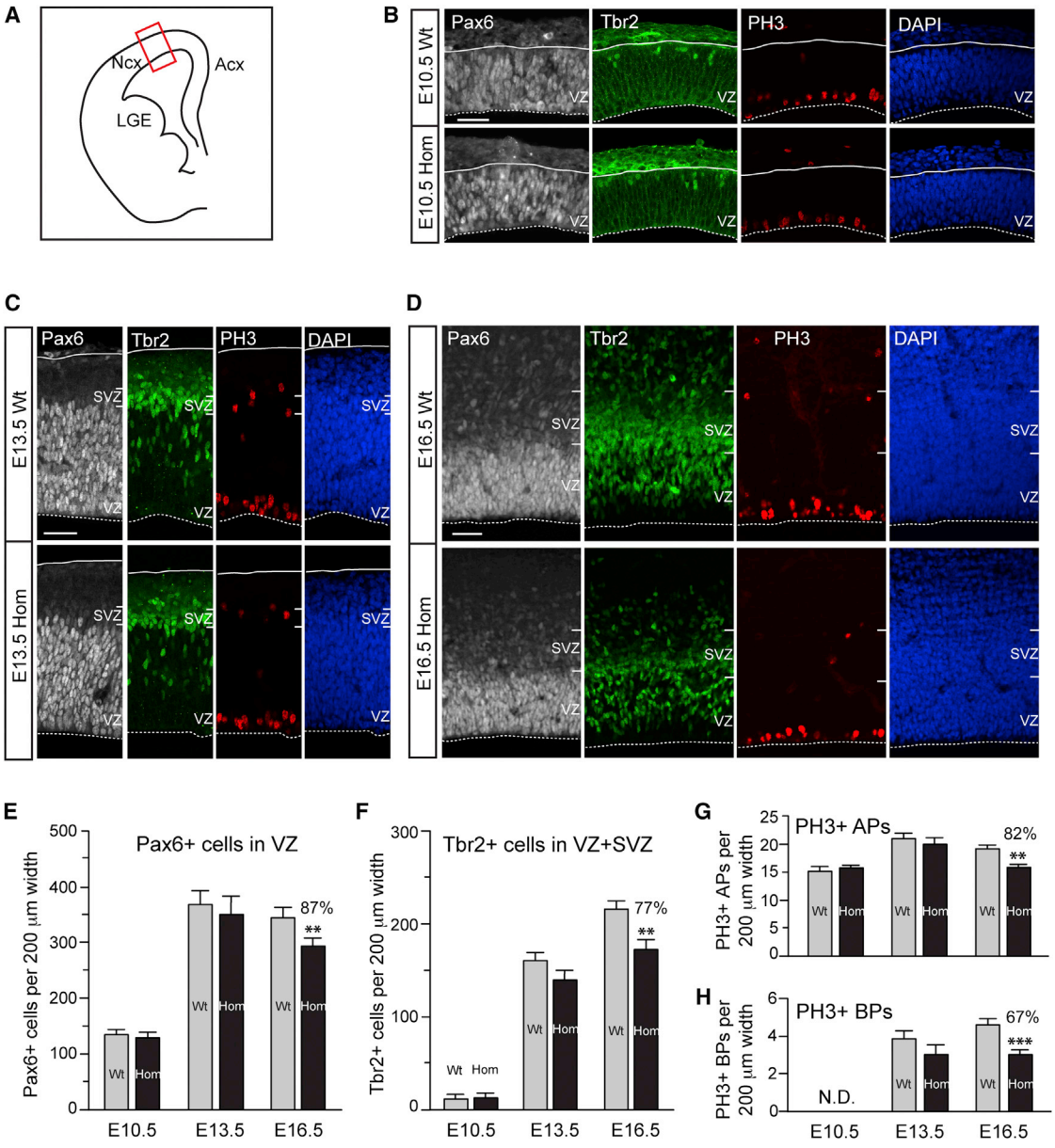

Figure 6. APs and BPs Are Reduced in KO Ncx at Late Neurogenesis

(A) Cartoon of coronal section of mouse E13.5 Tel showing the area of Ncx analyzed (red box). Acx, archicortex; LGE, lateral ganglionic eminence.

(B–D) IF for Pax6 (white), Tbr2 (green), and phospho-histone H3 (PH3, red) combined with DAPI staining (blue) on 10 μm coronal cryosections of E10.5 (B), E13.5 (C), and E16.5 (D) Ncx of WT (top) and hom KO (bottom) littermates. Tbr2 and PH3 are double IF, together with DAPI staining, on the same cryosections; each Pax6 staining is a separate IF. Solid white lines, basal lamina; dashed white lines, ventricular surface. Scale bars, 50 μm.

(E–H) Quantification of Pax6+ nuclei in VZ (E), Tbr2+ nuclei in VZ plus SVZ (F), apical PH3+ mitoses (G), and basal PH3+ mitoses (H), in each case in a 200-μm-wide field of E10.5 (left columns), E13.5 (middle columns), and E16.5 (right columns) Ncx of WT (gray columns) and hom KO (black columns) embryos. Mean of six determinations each (three embryos each, two cryosections per embryo); error bars, SEM; $^{**}p < 0.01$; $^{***}p < 0.001$. Numbers above columns: for each marker, mean WT value was set to 100%, and mean hom value is expressed relative to this.

neocortical APs of E15.5 WT and hom KO embryos with a plasmid encoding cytoplasmic GFP under the control of a constitutive promoter and analyzed GFP-expressing cells in the VZ and SVZ 12 hr and 20 hr after electroporation for the presence of proliferating cell nuclear antigen (PCNA; a marker of cycling cells) and Tbr2 immunoreactivity.

At 12 hr after electroporation, 47% and 53% of all GFP-expressing cells in the VZ plus SVZ of WT and hom KO Ncx, respectively, were PCNA+ and Tbr2+, i.e., newborn BPs (Figures 7G and 7H). At this time point, PCNA− cells, presumably newborn neurons, accounted for 9% and 10% of all GFP-expressing cells in the VZ plus SVZ of WT and hom KO Ncx,

respectively (Figures 7G and 7H). We considered these data in light of the observation that at E16.5, the neurogenic/BP-genic subpopulation of APs is reduced by about one-quarter to one-third in hom KO Ncx compared to WT (Figures 6E and 6G). Thus, the findings that upon GFP electroporation of APs at least the same percentage of GFP-expressing cells are newborn BPs in hom KO Ncx as in WT 12 hr later (Figure 7H, black columns) implies that a substantial proportion of the BP-genic APs had switched from ASD to SCD. Interestingly, concomitant with this switch, the ratio of newborn BPs in SVZ to VZ at 12 hr after electroporation was ~1:1 for hom KO Ncx and ~1:3 for WT Ncx (Figure 7J), indicating that at this time point, a much greater proportion of newborn BPs had migrated to the SVZ in the former than the latter.

Similarly, our data (Figure 7H, gray columns) imply that in hom KO Ncx, a substantial proportion of APs had switched from neurogenic (rather than BP-genic) ASD to SCD. However, in line with previous studies (Attardo et al., 2008), this so-called direct neurogenesis was relatively minor compared to the indirect neurogenesis via neurogenic BPs (Figure 7H).

The same findings in principle, showing a very similar percentage of GFP-expressing cells being either newborn BPs or newborn neurons for WT and hom KO Ncx, were made 20 hr after electroporation (Figure 7I). However, at this time point, the proportion of newborn neurons relative to that of newborn BPs had increased, presumably because some of the GFP-expressing neurogenic BPs had already generated neurons during the 20 hr time period. No difference in the ratio of newborn BPs in SVZ to VZ was observed for WT and hom KO Ncx at this time point (Figure 7K). Taken together, these observations are consistent with the notion that the Tis21 upregulation in neocortical APs of KO embryos causes a proportion of them to prematurely switch from BP-genic ASD to SCD, resulting in their progressive depletion and, consequently, the progressive reduction in the neurogenic BP pool size and in the amount of neurogenesis.

To obtain direct evidence in support of this notion, we electroporated neocortical APs of E15.5 WT and hom KO embryos with GFP as above and analyzed, 12 hr after electroporation, daughter cell pairs in the VZ (identified as described in the Supplemental Experimental Procedures) that had arisen from an AP division for the presence of PCNA and Tbr2 immunoreactivity. Three types of daughter cell pairs with NSPC identity were observed: (1) AP (PCNA+, Tbr2−) + AP (PCNA+, Tbr2−) (Figure 7L, left); (2) AP (PCNA+, Tbr2−) + BP (PCNA+, Tbr2+) (Figure 7L, middle); and (3) BP (PCNA+, Tbr2+) + BP (PCNA+, Tbr2+) (Figure 7L, right). Quantification of the two types of daughter cell pairs that reflected BP-genic divisions, that is, AP + BP (reflecting ASD) and BP + BP (reflecting SCD), showed that in WT only 24% of AP divisions were symmetric consumptive, whereas this was the case for 43% of the AP divisions in hom KO Ncx (Figure 7M). We conclude that Tis21 upregulation in APs of KO Ncx causes a fraction of these cells to switch from BP-genic ASD to SCD.

Posttranscriptional Upregulation of Tis21 at Late Neocortical Neurogenesis

As is described in detail in the Supplemental Results, Tis21 expression in the Tis21-positive cells increased at late neurogenesis (E16.5; Figures S4A and S4B). This likely was due, at least in part, to the increased expression of *Tis21* splice variants lacking most of the 3′ UTR (Figures S4C–S4E). Hence, a posttranscriptional upregulation of Tis21 expression in the Tis21-positive cells may contribute to the increase in AP SCDs that occurs at late neurogenesis.

DISCUSSION

Our study reveals a cause of microcephaly due to aberrant regulation at the level of NSCs. In the present form of microcephaly, the Ncx is more affected than other parts of the brain and the smaller size of the Ncx is primarily due to a decrease in radial thickness, with upper-layer neurons being more strongly reduced in number than deep-layer neurons. This phenotype results from the progressive depletion of neurogenic APs and, consequently, neurogenic BPs. Importantly, this depletion is caused by the lack of microRNA-mediated, 3′ UTR-dependent restriction of Tis21 expression in neurogenic APs, which changes the mode of AP division in vivo, rather than inhibiting cell-cycle progression as previously thought based on in vitro studies (Matsuda et al., 2001; Tirone, 2001).

The 3′ UTR-dependent restriction of Tis21 expression was found to be mediated by microRNAs, notably miR-92. Evidence for this is provided by the findings that the *Tis21-fl* mRNA, but not the *Tis21* mRNA lacking the 3′ UTR, is increased in Dicer-ablated d-Tel. In addition, fusion of the *Tis21* 3′ UTR to *mRFP* causes a massive decrease in mRFP expression, and removal not only of all 17 predicted microRNA target sites (Figure 3A) from the 3′ UTR but also of just the two miR-92 target sites reverses this decrease. Moreover, a miR-92 inhibitor, but not a microRNA inhibitor control, blocked the decrease in mRFP expression caused by fusion of the *Tis21* 3′ UTR to *mRFP*. The level of miR-92 has been reported to decrease during neurogenesis but at late neurogenesis is still about half of that at early neurogenesis (Miska et al., 2004; Bian et al., 2013). Hence, microRNA-mediated, 3′ UTR-dependent restriction of Tis21 expression from *Tis21-fl* mRNA is likely to occur, in principle, both at the early and late stages of neurogenesis, and so 3′UTR deletion would be expected to result in increased in Tis21 expression throughout neurogenesis.

How, then, does the increase in Tis21 expression in the neurogenic subpopulation of NSPCs upon 3′ UTR deletion cause the observed decrease in APs and BPs at E16.5? Our data indicate that in E16 KO Ncx, BP-genic SCDs of APs are increased at the expense of BP-genic ASDs. A possible explanation for this increase would be that inheritance of the Tis21 protein contributes to a BP fate and that the massively increased level of Tis21 protein in neocortical KO APs leads to a BP fate of both daughter cells. The exact mechanism of how Tis21 overexpression influences daughter cell fate remains to be elucidated. A switch of a fraction of neocortical KO APs from BP-genic ASDs to SCD would result in the progressive depletion of APs during the course of neurogenesis and, consequently, in the progressive reduction of the neurogenic BP pool size. This in turn would progressively reduce the number of neurons generated during neurogenesis. Moreover, such a cumulative effect upon 3′ UTR deletion is further amplified, at late neurogenesis, by the fact

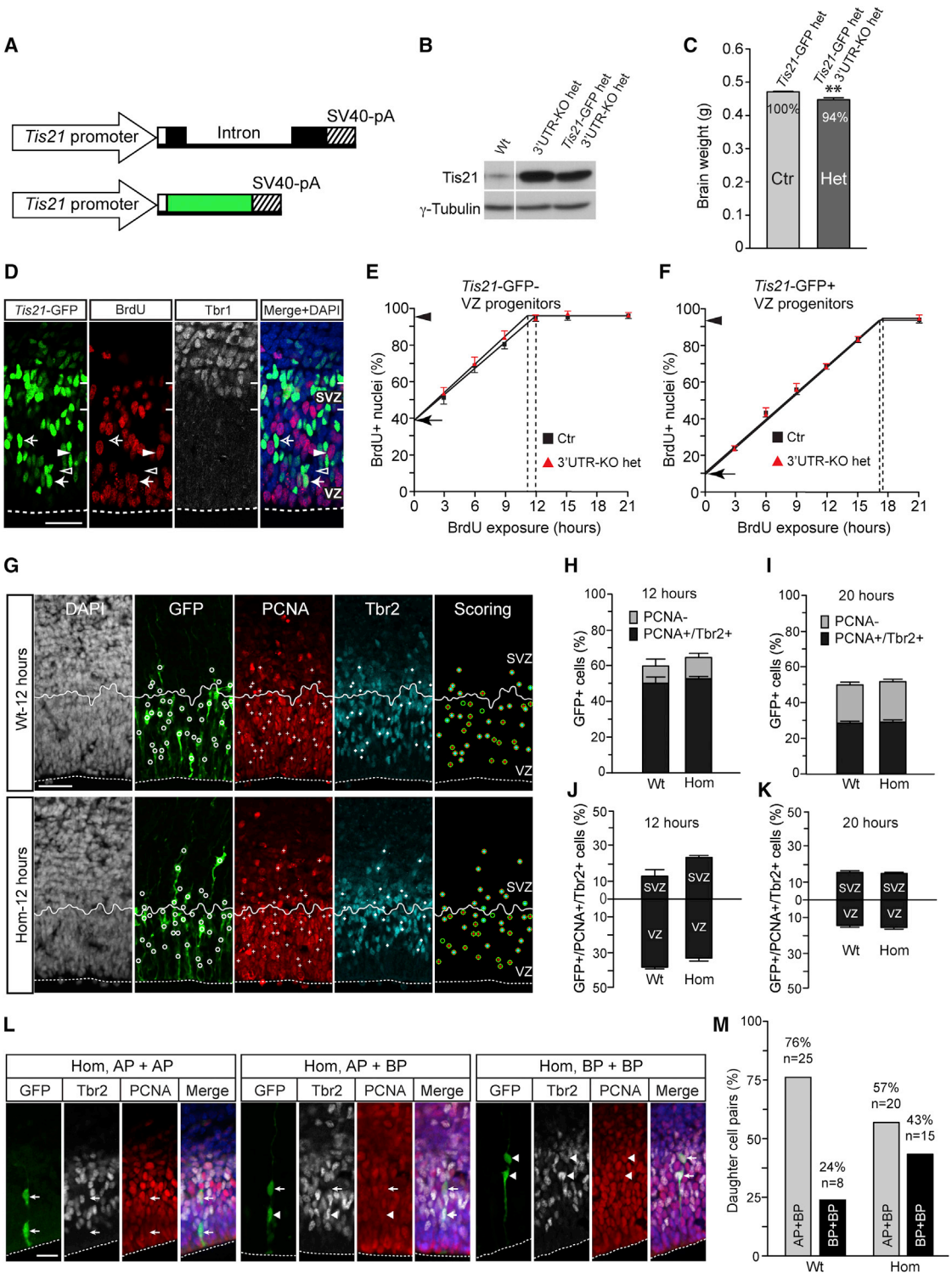

Figure 7. Tis21 Upregulation in Neurogenic NSPCs in VZ of KO Ncx Does Not Lengthen Their Cell Cycle but Increases Consumptive AP Divisions

(A) KO *Tis21* allele (top) and *Tis21*-GFP knockin allele (bottom).

(B) Tis21 immunoblot of WT, het KO, and double het *Tis21*-GFP/KO E13.5 brain (30 μg total protein). γ-Tubulin immunoblot, loading control. For each antigen, all three lanes are from the same immunoblot and exposure.

(legend continued on next page)

that the proportion of NSCs that express Tis21 increases from E10.5 to E16.5 (Haubensak et al., 2004). Given that upper-layer neurons are known to be generated later during neurogenesis than deep-layer neurons (Molyneaux et al., 2007), these considerations explain why, at birth, the former are more strongly reduced in number than the latter.

The observed increase in the fraction of KO APs undergoing BP-genic SCD provides a mechanistic explanation for the previously reported "antiproliferative" role of Tis21 (Matsuda et al., 2001; Tirone, 2001), at least with regard to NSCs. In these cells, as revealed by cumulative BrdU labeling, and contrary to a previous report (Canzoniere et al., 2004), the massively increased Tis21 level does not inhibit cell-cycle progression, nor does it cause cell-cycle arrest. Rather, any "antiproliferative" effect of Tis21 overexpression is an indirect consequence and reflects the change in the mode of NSC division (in line with a previous in vitro study; Malatesta et al., 2000) such that both daughter cells (rather than only one) become a neurogenic BP, which has the intrinsic property of undergoing only one terminal cell division that generates two postmitotic neurons.

The present microcephaly caused by increased Tis21 expression in KO mice differs with regard to not only the mechanism (see above) but also cell-type specificity from the small-brain phenotype previously observed upon inducible overexpression of PC3, the rat ortholog of Tis21, in mice (Canzoniere et al., 2004). First, the latter small-brain phenotype was reported when a constitutive promoter (β-actin) was used. Second, this previous phenotype was accompanied by increased apoptosis in germinal zones, which was not observed in the present study. Third, increased neurogenesis in the neural tube and cerebellum, but no smaller cerebral cortex, was reported when PC3 was overexpressed using the nestin promoter (Canzoniere et al., 2004), which is known to drive gene expression in virtually all (not only neurogenic) APs and not in BPs. In contrast, our study shows that (1) Tis21 overexpression in the Ncx was restricted to those cells that physiologically express the *Tis21* gene, that is, the neurogenic subpopulations of NSPCs (Haubensak et al., 2004; Iacopetti et al., 1999), and (2) Tis21 overexpression is shown to alter the mode of cell division in vivo, rather than cell-cycle progression.

Our findings identify the 3′ UTR as a major regulatory element that curtails the level of Tis21 expression in APs, a constraint essential to sustain the ability of these cells to undergo repeated BP-genic ASDs. This regulation is likely to be relevant in the context of Ncx development, because the Tis21 protein level in *Tis21*-expressing cells was more than twice as high at E16.5 than at E13.5 and E10.5. At this late stage of mouse neurogenesis, there is an increase in APs switching from ASD to SCD, and the higher cellular Tis21 protein level may contribute to this switch. As to the cause of this increase in the cellular Tis21 level at E16.5, at least two possibilities exist. One is the increased contribution of 3′ UTR-truncated splice variants, which are less likely to be subject to microRNA-induced mRNA degradation than the *Tis21-fl* mRNA, to the total *Tis21* mRNA toward the end of cortical neurogenesis.

Another, not mutually exclusive, possibility is a change in the level of specific microRNAs during neurogenesis. Specifically, concomitant with the rise in the cellular Tis21 protein level toward the end of cortical neurogenesis, the expression of miR-17 and miR-92, for which there are one and two predicted binding sites, respectively, in the *Tis21* 3′ UTR, in the embryonic rodent Ncx is reduced (Miska et al., 2004; Yao et al., 2012). Thus, miR-17 and miR-92, which have recently been shown to be expressed in APs (Bian et al., 2013), emerge as candidate microRNAs to curtail, via the 3′ UTR, the level of Tis21 expression during early and mid-neurogenesis. Interestingly, and fully consistent with the present observations, a very recent study has shown that conditional deletion of the miR-17∼92 cluster in the developing mouse Ncx promotes the transition of APs to neurogenic BPs (Bian et al., 2013). Moreover, the miR-17∼92 cluster has been

(C) Brain weight of adult (9–13 weeks old) het *Tis21*-GFP (Ctr, light gray) and double het *Tis21*-GFP/KO mice (dark gray). Mean of 13 (Ctr) and 15 (Het) determinations; error bars, SEM; **$p < 0.01$. Numbers: mean control value was set to 100%, and mean double het value is expressed relative to this.

(D) An E14.5 het *Tis21*-GFP embryo was labeled by a single pulse of BrdU in utero, followed 3 hr later by triple IF for *Tis21*-GFP (green), BrdU (red), and Tbr1 (white) combined with DAPI staining (blue) on a 10 μm coronal cryosection of Ncx. Examples of *Tis21*-GFP−/BrdU+ (solid arrowhead), *Tis21*-GFP−/BrdU− (open arrowhead), *Tis21*-GFP+/BrdU+ (solid arrow), and *Tis21*-GFP+/BrdU− (open arrow) nuclei in VZ are indicated. Dashed lines, ventricular surface. Scale bar, 50 μm.

(E and F) Cumulative BrdU labeling for up to 21 hr of *Tis21*-GFP− (E) and *Tis21*-GFP+ (F) NSPCs in E14.5 het *Tis21*-GFP (Ctr, black squares) and double het *Tis21*-GFP / KO (3′UTR-KO het, red triangles) Ncx VZ. Mean of eight determinations each (four embryos from two independent litters each, two cryosections per embryo) except for (9 hr in E and 6 hr in F, three embryos from two litters); error bars, SEM. Horizontal lines and arrowheads, growth fraction; arrows, proportion of NSPCs in S phase; vertical dashed lines, time interval between two consecutive S phases ($T_C - T_S$).

(G–M) dl-Tel of WT (G top) and hom KO (G bottom) E15.5 littermates was electroporated with pCAGGS-*EGFP* and analyzed 12 hr (G, H, J, L, and M) or 20 hr (I and K) later.

(G) Triple IF for GFP (green), PCNA (red), and Tbr2 (cyan) combined with DAPI staining (white) on 50 μm coronal vibratome sections (4 μm optical sections). Circles, GFP+ cells; crosses, PCNA+ cells; diamonds, Tbr2+ cells; merged symbols facilitating scoring of cells are shown in the right panels. Dashed lines, ventricular surface; solid lines, VZ-SVZ boundary. Scale bar, 50 μm.

(H and I) Quantification of GFP+/PCNA+/Tbr2+ (black columns) and GFP+/PCNA− (gray columns) cells in VZ plus SVZ, expressed as percentage of total GFP+ cells.

(J and K) Distribution of GFP+/PCNA+/Tbr2+ cells between VZ (below 0 line) and SVZ (above 0 line), using the percentage values shown in (H) and (I), respectively.

(H–K) Mean of three (WT 12 hr), four (hom 12 hr), eight (WT 20 hr), and eight (hom 20 hr) cryosections scored; error bars, SEM.

(L) Examples of daughter cell pairs derived from hom KO AP divisions; triple IF for GFP (green), Tbr2 (white), and PCNA (red) combined with DAPI staining (blue) on 50 μm coronal vibratome sections (4 μm optical sections). (Left) AP (PCNA+, Tbr2−) + AP (PCNA+, Tbr2−); (middle) AP (PCNA+, Tbr2−) + BP (PCNA+, Tbr2+); (right) BP (PCNA+, Tbr2+) + BP (PCNA+, Tbr2+); arrows, APs; arrowheads, BPs; dotted lines, ventricular surface. Scale bar, 20 μm.

(M) Quantification of AP + BP (gray columns) and BP + BP (black columns) daughter cell pairs arising from BP-genic ASDs and SCDs of APs, respectively. Data were collected from seven WT and eight hom KO embryos of four litters; numbers of daughter cell pairs are indicated. For either WT or hom, the AP + BP and BP + BP pairs are expressed as percentage of the sum of AP + BP plus BP + BP pairs.

reported to be deleted in humans with microcephaly (de Pontual et al., 2011). This provides a remarkable parallel to the microcephaly of the *Tis21* 3′ UTR mutant mice reported in the present study that results from the lack of microRNA-dependent regulation of Tis21 expression.

Taken together, our study demonstrates that specific microRNAs, notably miR-92, that are known to be downregulated toward the end of neurogenesis, restrict Tis21 expression via its 3′ UTR and thereby ensure the maintenance of repeated self-renewing divisions of neurogenic/BP-genic APs. These findings provide insight into how the length of the neurogenic phase of a given AP is controlled. Our study therefore contributes to understanding the timing of cessation of neurogenesis, a fundamental parameter of Ncx development and evolution.

EXPERIMENTAL PROCEDURES

For further details, see the Supplemental Experimental Procedures. All other methods were carried out according to established protocols.

DNA Constructs

All plasmid constructs were generated using standard molecular cloning techniques. The targeting construct for homologous recombination in embryonic SCs, p15A-3′ UTR-KO-*neo* (Figure S1H, i), was generated from the BAC bMQ-284G14 using the Red/ET homologous recombination technology.

Mouse Lines

The 3′ UTR-KO mouse line was generated by standard techniques, using the ESC clone #46C carrying a 3′ UTR-KO-*neo* allele (Figure S1H, iii), crossing the 3′ UTR-KO-*neo* F1 progeny with *hACTB*-FLPe mice to remove the neomycin cassette and backcrossing with C57BL/6J mice. All animal experiments were performed in accordance with German animal welfare legislation.

Quantifications

Length of Ncx ventricular and pial surfaces and radial thickness were determined on fluorescence images using Fiji and AxioVision software. Cell-cycle parameters after cumulative BrdU labeling were calculated as described previously (Arai et al., 2011). Daughter cell pairs were identified based on the spatial pattern of GFP-expressing cells and level of GFP expression. Plotting of data and statistical analyses were performed using Microsoft Excel and "R," respectively. Student's t test was used for the calculation of p values.

SUPPLEMENTAL INFORMATION

Supplemental Information includes Supplemental Results, Supplemental Discussion, Supplemental Experimental Procedures, and four figures and can be found with this article online at http://dx.doi.org/10.1016/j.celrep.2014.03.033.

ACKNOWLEDGMENTS

We are indebted to various services and facilities of the Max Planck Institute of Molecular Cell Biology and Genetics for outstanding support, notably Jussi Helppi and his team at the Animal Facility, Ronald Naumann and his team at the Transgenic Core Facility, and Sylke Winkler and her team at the DNA Sequencing Facility. pCAGGS-*EGFP* was a kind gift of Dr. Elly Tanaka. We thank Drs. Davide De Pietri Tonelli, Jeremy Pulvers, and Elena Taverna for helpful discussions and advice. J.-F.F. was a member of the International Max Planck Research School for Molecular Cell Biology and Bioengineering and a doctoral student at the Technische Universität Dresden. W.B.H. was supported by grants from the Deutsche Forschungsgemeinschaft (DFG) (SFB 655, A2; TRR 83, Tp6) and the European Research Council (250197), by the DFG-funded Center for Regenerative Therapies Dresden, and by the Fonds der Chemischen Industrie.

Received: August 19, 2013
Revised: January 9, 2014
Accepted: March 9, 2014
Published: April 10, 2014

REFERENCES

Arai, Y., Pulvers, J.N., Haffner, C., Schilling, B., Nüsslein, I., Calegari, F., and Huttner, W.B. (2011). Neural stem and progenitor cells shorten S-phase on commitment to neuron production. Nat Commun *2*, 154.

Attardo, A., Calegari, F., Haubensak, W., Wilsch-Bräuninger, M., and Huttner, W.B. (2008). Live imaging at the onset of cortical neurogenesis reveals differential appearance of the neuronal phenotype in apical versus basal progenitor progeny. PLoS ONE *3*, e2388.

Bian, S., Hong, J., Li, Q., Schebelle, L., Pollock, A., Knauss, J.L., Garg, V., and Sun, T. (2013). MicroRNA cluster miR-17-92 regulates neural stem cell expansion and transition to intermediate progenitors in the developing mouse neocortex. Cell Rep *3*, 1398–1406.

Borrell, V., and Reillo, I. (2012). Emerging roles of neural stem cells in cerebral cortex development and evolution. Dev. Neurobiol. *72*, 955–971.

Bradbury, A., Possenti, R., Shooter, E.M., and Tirone, F. (1991). Molecular cloning of PC3, a putatively secreted protein whose mRNA is induced by nerve growth factor and depolarization. Proc. Natl. Acad. Sci. USA *88*, 3353–3357.

Canzoniere, D., Farioli-Vecchioli, S., Conti, F., Ciotti, M.T., Tata, A.M., Augusti-Tocco, G., Mattei, E., Lakshmana, M.K., Krizhanovsky, V., Reeves, S.A., et al. (2004). Dual control of neurogenesis by PC3 through cell cycle inhibition and induction of Math1. J. Neurosci. *24*, 3355–3369.

Chen, C.Y., and Shyu, A.B. (1995). AU-rich elements: characterization and importance in mRNA degradation. Trends Biochem. Sci. *20*, 465–470.

De Pietri Tonelli, D., Pulvers, J.N., Haffner, C., Murchison, E.P., Hannon, G.J., and Huttner, W.B. (2008). miRNAs are essential for survival and differentiation of newborn neurons but not for expansion of neural progenitors during early neurogenesis in the mouse embryonic neocortex. Development *135*, 3911–3921.

de Pontual, L., Yao, E., Callier, P., Faivre, L., Drouin, V., Cariou, S., Van Haeringen, A., Geneviève, D., Goldenberg, A., Oufadem, M., et al. (2011). Germline deletion of the miR-17∼92 cluster causes skeletal and growth defects in humans. Nat. Genet. *43*, 1026–1030.

Englund, C., Fink, A., Lau, C., Pham, D., Daza, R.A., Bulfone, A., Kowalczyk, T., and Hevner, R.F. (2005). Pax6, Tbr2, and Tbr1 are expressed sequentially by radial glia, intermediate progenitor cells, and postmitotic neurons in developing neocortex. J. Neurosci. *25*, 247–251.

Fietz, S.A., and Huttner, W.B. (2011). Cortical progenitor expansion, self-renewal and neurogenesis-a polarized perspective. Curr. Opin. Neurobiol. *21*, 23–35.

Fletcher, B.S., Lim, R.W., Varnum, B.C., Kujubu, D.A., Koski, R.A., and Herschman, H.R. (1991). Structure and expression of TIS21, a primary response gene induced by growth factors and tumor promoters. J. Biol. Chem. *266*, 14511–14518.

Götz, M., and Huttner, W.B. (2005). The cell biology of neurogenesis. Nat. Rev. Mol. Cell Biol. *6*, 777–788.

Haubensak, W., Attardo, A., Denk, W., and Huttner, W.B. (2004). Neurons arise in the basal neuroepithelium of the early mammalian telencephalon: a major site of neurogenesis. Proc. Natl. Acad. Sci. USA *101*, 3196–3201.

Huntzinger, E., and Izaurralde, E. (2011). Gene silencing by microRNAs: contributions of translational repression and mRNA decay. Nat. Rev. Genet. *12*, 99–110.

Iacopetti, P., Michelini, M., Stuckmann, I., Oback, B., Aaku-Saraste, E., and Huttner, W.B. (1999). Expression of the antiproliferative gene TIS21 at the onset of neurogenesis identifies single neuroepithelial cells that switch from proliferative to neuron-generating division. Proc. Natl. Acad. Sci. USA *96*, 4639–4644.

Jalava, S.E., Urbanucci, A., Latonen, L., Waltering, K.K., Sahu, B., Jänne, O.A., Seppälä, J., Lähdesmäki, H., Tammela, T.L., and Visakorpi, T. (2012). Androgen-regulated miR-32 targets BTG2 and is overexpressed in castration-resistant prostate cancer. Oncogene *31*, 4460–4471.

Kowalczyk, T., Pontious, A., Englund, C., Daza, R.A., Bedogni, F., Hodge, R., Attardo, A., Bell, C., Huttner, W.B., and Hevner, R.F. (2009). Intermediate neuronal progenitors (basal progenitors) produce pyramidal-projection neurons for all layers of cerebral cortex. Cereb. Cortex *19*, 2439–2450.

Kriegstein, A., and Alvarez-Buylla, A. (2009). The glial nature of embryonic and adult neural stem cells. Annu. Rev. Neurosci. *32*, 149–184.

Lai, E.C., and Posakony, J.W. (1997). The Bearded box, a novel 3′ UTR sequence motif, mediates negative post-transcriptional regulation of Bearded and Enhancer of split Complex gene expression. Development *124*, 4847–4856.

Lui, J.H., Hansen, D.V., and Kriegstein, A.R. (2011). Development and evolution of the human neocortex. Cell *146*, 18–36.

Malatesta, P., Götz, M., Barsacchi, G., Price, J., Zoncu, R., and Cremisi, F. (2000). PC3 overexpression affects the pattern of cell division of rat cortical precursors. Mech. Dev. *90*, 17–28.

Matsuda, S., Rouault, J., Magaud, J., and Berthet, C. (2001). In search of a function for the TIS21/PC3/BTG1/TOB family. FEBS Lett. *497*, 67–72.

Miska, E.A., Alvarez-Saavedra, E., Townsend, M., Yoshii, A., Sestan, N., Rakic, P., Constantine-Paton, M., and Horvitz, H.R. (2004). Microarray analysis of microRNA expression in the developing mammalian brain. Genome Biol. *5*, R68.

Molyneaux, B.J., Arlotta, P., Menezes, J.R., and Macklis, J.D. (2007). Neuronal subtype specification in the cerebral cortex. Nat. Rev. Neurosci. *8*, 427–437.

Murchison, E.P., Partridge, J.F., Tam, O.H., Cheloufi, S., and Hannon, G.J. (2005). Characterization of Dicer-deficient murine embryonic stem cells. Proc. Natl. Acad. Sci. USA *102*, 12135–12140.

Rakic, P. (2009). Evolution of the neocortex: a perspective from developmental biology. Nat. Rev. Neurosci. *10*, 724–735.

Rouault, J.P., Falette, N., Guéhenneux, F., Guillot, C., Rimokh, R., Wang, Q., Berthet, C., Moyret-Lalle, C., Savatier, P., Pain, B., et al. (1996). Identification of BTG2, an antiproliferative p53-dependent component of the DNA damage cellular response pathway. Nat. Genet. *14*, 482–486.

Tirone, F. (2001). The gene PC3(TIS21/BTG2), prototype member of the PC3/BTG/TOB family: regulator in control of cell growth, differentiation, and DNA repair? J. Cell. Physiol. *187*, 155–165.

Yang, C.H., Yue, J., Pfeffer, S.R., Handorf, C.R., and Pfeffer, L.M. (2011). MicroRNA miR-21 regulates the metastatic behavior of B16 melanoma cells. J. Biol. Chem. *286*, 39172–39178.

Yao, M.J., Chen, G., Zhao, P.P., Lu, M.H., Jian, J., Liu, M.F., and Yuan, X.B. (2012). Transcriptome analysis of microRNAs in developing cerebral cortex of rat. BMC Genomics *13*, 232.